

Research article

# Lignin-liquid crystalline elastomeric composites for shape memory applications and their thermomechanical properties

Peerawat Prathumrat<sup>1</sup>, Mostafa Nikzad<sup>1\*</sup>, Elnaz Hajizadeh<sup>2</sup>, Manunya Okhawilai<sup>3</sup>,  
Igor Sbarski<sup>1</sup>

<sup>1</sup>Department of Mechanical and Product Design Engineering, School of Engineering, Swinburne University of Technology, 3122 Hawthorn, VIC, Australia

<sup>2</sup>Department of Mechanical Engineering, Faculty of Engineering and Information Technology, University of Melbourne, 3010 Parkville, VIC, Australia

<sup>3</sup>Metallurgy and Materials Science Research Institute, Chulalongkorn University, Pathumwan, 10330 Bangkok, Thailand

Received 4 June 2022; accepted in revised form 27 August 2022

**Abstract.** Liquid crystalline elastomers (LCEs) are stimuli-responsive materials with potential use in shape memory applications. Though particularly suited for shape memory, the LCEs however have some drawbacks such as low shape fixity ( $R_f$ ) and slow recovery time. To overcome these limitations, new lignin-filled elastomeric liquid crystalline (ELC) composite materials were fabricated. The lignin used is a by-product of Kraft pulping process, which was obtained from renewable resources abundant in nature. Here, we show that the aromatic structure of lignin increases the netpoints density at the microscopic level in the ELC composite systems. Shape memory effects are enhanced by incorporating up to only 7 wt% of lignin, resulting in an  $R_f$  of 97% for the composites. Concurrently, these composites were able to maintain their shape recovery ( $R_r$ ) of nearly 100%. The recovery time of the composites reduces with increasing lignin content due to the higher elastic energy released from the netpoints based on the lignin structure. The ELC composites with 7 wt% lignin could fully recover within 70 s, while the neat LCE counterpart took 100 s. Morphological features of dispersed lignin shows that even without surface modification and only a moderate quality of dispersion in LCE matrix, both shape memory and dynamic mechanical properties of the resultant composites can be significantly improved.

**Keywords:** smart materials, shape memory elastomers (SMEs), liquid crystalline elastomers (LCEs), lignin, composites

## 1. Introduction

Shape memory elastomers (SMEs) are a class of intelligent materials that have been utilized over the past decades in a wide range of applications, such as soft robotics, aerospace engineering, smart actuators and sensors, and biomedical devices [1–4]. These materials have the ability to deform and memorize their temporary shape and eventually recover to their original shape under applied stress and an external stimulus. Several external stimuli are currently used to activate the shape memory effects of polymeric

systems, such as heat, UV, electric and magnetic fields, water, and pH [5]. Among them, heat is commonly used for activation [6, 7]. The molecular architecture of the elastomer also plays a critical role in allowing the material to exhibit shape memory effects [8, 9]. The SMEs typically consist of two prerequisite constituents, including netpoints and switch units. The netpoints (hard segments) are responsible for determining the original shape of the SMEs due to their ability to store the elastic energy during the shape memory process [10]. This segment can also

\*Corresponding author, e-mail: [mnikzad@swin.edu.au](mailto:mnikzad@swin.edu.au)

© BME-PT

help SMEs to maintain their temporary shape due to their chemical or physical crosslinks or interpenetrated networks (IPNs). The switch units (soft segments) are responsible for maintaining the temporary shape and recovering the original shape through transition temperatures [11]. A well-balanced proportion of these constituents can lead to an excellent shape memory performance via thermomechanical shape memory processes.

Liquid crystalline elastomers (LCEs) are stimuli-responsive materials that have gained increasing attention for their potential shape memory effects [12, 13]. The molecular structure of LCEs consists of mesogens (hard segment) and flexible tails (soft segment), allowing them to possess the typical underlying molecular mechanism of SMEs [8]. These materials can also respond to many external stimuli via the shape deformation process [12, 14–16]. The LCEs typically exhibit two transition temperatures: glass transition temperature ( $T_g$ ) and nematic-isotropic transition temperature ( $T_{NI}$ ). These transition temperatures allow the LCE structure to rearrange from solid-crystal to liquid-crystal and isotropic states. In the shape memory mechanism of LCEs,  $T_{NI}$  is utilized as a switching point because it is higher than room temperature, resulting in no interruptions from ambient conditions.

Reactive mesogens (RM)-based LCE have become a crucial nematic-LCE for SMEs [17, 18]. This class of LCEs can be thermally stimulated to mobilize its networks via a nematic-isotropic transition temperature ( $T_{NI}$ ) [19]. Traugutt *et al.* [20] have studied the effect of solvent used in the synthesis process on shape memory properties of RM257-based LCE. The results showed that the shape fixity ( $R_f$ ) and the shape recovery ( $R_r$ ) of the case with solvent was approximately 62.8 and 99.5%, respectively. These properties were higher than the case without the solvent. Guin *et al.* [21] have reported that combining two reactive (diacrylate) mesogens, RM82 and RM257, in the LCE system results in an excellent thermal actuation up to 11 cycles, provided that the LCE structure remains stable and can maintain an actuation behavior through thermal deformation processes.

Other LCE systems have also been developed to study the shape memory effects. Wen *et al.* [22] synthesized a multiple-shape memory LCE from a novel polyurethane with exchangeable carbamate functional groups. This LCE system indicated two liquid crystal phases, including smectic-A and nematic,

showing two transition temperatures: smectic-nematic transition temperature ( $T_{SmN}$ ) and nematic-isotropic transition temperature ( $T_{NI}$ ). As a result, these materials showed the  $R_f$  of 84.5 and 88.6% for the first and second temporary shapes and an outstanding  $R_r$  of 99% for both shapes. Rousseau and Mather [23] studied the shape memory properties of main-chain smectic-C LCE synthesized by benzoate mesogenic groups. This LCE revealed an  $R_f$  of 83.6% and an excellent  $R_r$  of 99.1% via a thermal-induced process.

These reported works on neat LCEs show their excellent potential as candidates for shape memory materials and possessing a significant  $R_r$  characteristic. However, there seems to be a shortcoming in achieving full  $R_r$  using these LCEs systems, and importantly that all the critical compounds used in their preparation produced from non-renewable sources and hence limiting their applications for large and high-volume applications. It is also noteworthy to mention that currently available systems are synthesized from expensive compounds, making their wider uptake cost-prohibitive. Another key performance attribute that requires further improvement is the longer recovery time of shape memory applications developed from the existing homogenous LCE systems [24]. These shortcomings are some key barriers to the further adoption of these promising class of smart materials for the development of exotic industrial and space applications.

To address the aforementioned shortcomings and further improve the shape memory characteristics of LCEs, creating composites of LCE and naturally derived compounds such as lignin is one promising option. Thanks to the high concentration of aromatic compounds and the complex interconnect molecular structures of monolignols, often providing large surface areas, they can be incorporated as rigid fillers into the LCE matrix to provide synergistic effects not available in the existing homogenous systems, otherwise. These composite LCEs can therefore provide mitigation strategies for improved  $R_r$  and being abundant as well as renewably obtained, increase sustainability in terms of cost and scalability. An example of such lignin sources is obtained from Kraft pulping process as a by-product, which contributes to 85% of the total lignin manufacturing globally [25]. This biomaterial is a three-dimensional macromolecular polymer constructed from three different phenylpropane monomer units; p-coumaryl alcohol, coniferyl alcohol, and syringyl alcohol [26]. It has gained increasing

attention in many research areas due to its remarkable properties, including low cost, renewability, biodegradability, high thermal stability, anti-oxidation, and high UV absorption properties [27–29]. These properties also promote lignin as a significant natural resource fulfilling the global demand for other environmentally benign polymeric materials.

In shape memory applications, incorporating lignin into the shape memory polymeric systems increases the density of netpoints (hard segment) in the composites due to its networked phenolic structures and intermolecular hydrogen bonding [30]. These characteristics can enhance the  $R_f$  of the polymeric composites to approximately 100% [31]. This biomaterial can also improve the tensile modulus and strength of the composites, resulting in broadening areas of engineering applications [32, 33]. Moreover, the copolymeric structures of lignin-co-poly(ester-amine-amide) exhibited a triple-shape memory effect via a thermomechanical process [34]. Therefore, given an appropriate molecular structure of lignin, this material offers potential as a good filler in preparing LCE-based shape memory elastomeric composites with improved intrinsic properties, including dynamic mechanical and shape memory properties.

To achieve the desired characteristics in the shape memory applications, we considered the liquid crystalline elastomeric composites in which Kraft lignin-based bio-filler is added to diacrylate mesogens-based nematic LCE. This work focuses on the synthesis and characterization of new elastomeric liquid crystalline (ELC) composites with the goal of understanding how lignin improves shape memory properties and other underlying characteristics of composite materials. The nematic-type LCE was synthesized from diacrylate mesogens named RM257 and pentaerythritol tetra (3-mercaptopropionate) (PETMP) via a base-catalyzed thiol-Michael addition reaction. The lignin with different weight ratios was physically mixed to generate the ELC composites. The shape memory characteristics were measured, including  $R_f$ ,  $R_r$ , and recovery time. The effect of lignin filler is also studied on the thermal, dynamic mechanical, and morphological properties of the composites.

## 2. Experiments

### 2.1. Materials

The chemicals used in this study include diacrylate mesogen named 1,4-bis(4-(3-acryloyloxypropyl)oxy)benzoyl-oxy]-2-methylbenzene (RM257), which

was purchased from Daken Chemical (China). Kraft lignin (alkali lignin), pentaerythritol tetra (3-mercaptopropionate) (PETMP)-based crosslinking agent, and dipropyl amine (DPA)-based catalyst were purchased from Sigma-Aldrich, Inc. (Australia). Toluene was purchased from Thermo Fisher Scientific Australia PTY LTD (Australia). All these materials were used as received without further purification.

### 2.2. Sample preparation

The LCE samples were prepared following the same procedure reported in our previous work [17]. Briefly, RM257 monomers were dissolved by adding 40 wt% of toluene and heated at 80 °C in an oven until a homogenous solution was achieved. The solution was then left to cool down to room temperature. To develop composites, Kraft lignin was added at different mass ratios of 3, 5, and 7 wt% into the solution and was stirred until a well-dispersed mixture was achieved. In the next step, 36 wt% of PETMP was added to the system and stirred for several minutes. Dipropyl amine (DPA) was separately diluted in toluene at a mass ratio of 1:50, and subsequently, 14 wt% of the diluted DPA was added into the monomer mixture. All the constituents were instantaneously stirred and subsequently placed in a vacuum oven for 1 min to remove the bubble that occurred during mixing. The mixture was immediately transferred into the mold and left to cure at room temperature for 24 h. After the polymerization was completed, the LCE samples became glossy white and transparent elastomeric materials. Finally, the samples were heated to remove the solvent at 80 °C for 12 h before characterization. Figure 1 shows the molecular structure and the samples of all the monomers, LCE, and ELC composite after completing the synthesis process.

## 3. Characterization of LCE and composites

### 3.1. Fourier transform infrared spectroscopy (FTIR)

FTIR analysis was conducted on structural characterization of LC monomer (RM257), Kraft lignin, LCE, and ELC composite samples. The FTIR Nicolet iS5 (Thermo Scientific) was utilized to characterize the chemical compositions of the samples. The spectra were scanned in a transmittance mode with a scan range of 4000 to 400  $\text{cm}^{-1}$ , and the scan times were 64 scans per sample.

### 3.2. Thermal properties

A differential scanning calorimeter (DSC) 2960 (TA Instruments, USA) was employed to characterize the thermal properties of LCE and composite samples. The sample mass of 5 to 10 mg was used and sealed in an aluminum pan. The heating rate of  $5\text{ }^{\circ}\text{C}\cdot\text{min}^{-1}$  and cooling rate of  $3\text{ }^{\circ}\text{C}\cdot\text{min}^{-1}$  were set for running the sample in the temperature range of  $-40\text{ }^{\circ}\text{C}$  to  $150\text{ }^{\circ}\text{C}$ . The samples were run under an  $\text{N}_2$  atmosphere with a dispersed rate of  $110\text{ ml}\cdot\text{min}^{-1}$ . The phase transitions of LC monomer, LCE, and ELC composites were characterized.

A thermogravimetric analyzer (TGA) Q50 (TA Instruments, USA) was used to measure the thermal stability of the samples. The sample mass used was in the range of 10 to 20 mg. The testing temperature was ramped from 25 to  $800\text{ }^{\circ}\text{C}$  in the air with a heating rate of  $10\text{ }^{\circ}\text{C}\cdot\text{min}^{-1}$ . Thermal degradation temperatures and derivative thermogravimetric (DTG) curves of LCE and ELC composites were determined.

### 3.3. Dynamic mechanical properties

A discovery hybrid rheometer (DHR) HR-1 (TA Instruments, USA) was used for dynamic mechanical analysis (DMA) in a tensile mode. The dynamic mechanical properties of the LCE and ELC composites were measured in an oscillation procedure. The sample dimensions were  $30\times 6\times 1.2\text{ mm}^3$  for  $L\times W\times T$ . The temperature was ramped from  $-10$  to  $120\text{ }^{\circ}\text{C}$  with a heating rate of  $3\text{ }^{\circ}\text{C}\cdot\text{min}^{-1}$ . The axial displacement and frequency were set at  $25\text{ }\mu\text{m}$  and  $1\text{ Hz}$ , respectively. The storage modulus of LCE and ELC composites at nematic and isotropic states was measured using storage modulus curves at  $25$  and  $110\text{ }^{\circ}\text{C}$ , respectively. The nematic-isotropic temperatures ( $T_{\text{NI}}$ ) of all samples were determined from the second peak of the  $\tan\delta$ . This temperature was then used as a switching point in a shape memory process.

### 3.4. Shape memory properties

A DHR with a tensile mode was also used to evaluate the shape memory properties, including  $R_f$  and  $R_r$  of LCE and ELC composites. Shape memory testing was conducted via a four-step thermomechanical process under a stress-controlled condition. The sample was pre-heated at  $105\text{ }^{\circ}\text{C}$ , above its  $T_{\text{NI}}$ , and stretched with a  $5\%\cdot\text{min}^{-1}$  strain rate for 10 min. The sample was cooled down to  $25\text{ }^{\circ}\text{C}$  with a cooling rate of  $5\text{ }^{\circ}\text{C}\cdot\text{min}^{-1}$ . The force was unloaded, and the sample

was kept at  $25\text{ }^{\circ}\text{C}$  for 10 min. The sample was reheated at  $105\text{ }^{\circ}\text{C}$  to recover with a heating rate of  $5\text{ }^{\circ}\text{C}\cdot\text{min}^{-1}$  and kept at this temperature for 20 min. The  $R_f$  and  $R_r$  were calculated in the unloading and reheating steps by Equations (1) and (2):

$$R_f = \frac{\epsilon_i}{\epsilon_m} \cdot 100\% \quad (1)$$

$$R_r = \frac{\epsilon_m - \epsilon_p(n)}{\epsilon_m - \epsilon_p(n-1)} \cdot 100\% \quad (2)$$

where  $\epsilon_i$  is the residual strain in the unloading step after deformation,  $\epsilon_m$  is a maximum strain applied to the samples,  $\epsilon_p$  is the strain after recovery of the samples, and  $n$  is the number of cycles.

The recovery angle of LCE and ELC composites was measured as a function of time to study the effect of Kraft lignin on the recovery time of the specimens. The rectangular-shaped samples were preheated in an oven at  $105\text{ }^{\circ}\text{C}$  for 20 min. Then, they were deformed to a U-shape and cooled down to room temperature. The U-shaped samples were then put into an oven at  $105\text{ }^{\circ}\text{C}$ , where a degree protractor was set inside. A video camera was used to record the shape recovery behavior of these samples until they were completely reversed to a rectangular shape. This method was reported by Likitaporn *et al.* [35].

### 3.5. Scanning electron microscopy (SEM)

The surface morphology of the ELC composites fraction was studied using a scanning electron microscope (Zeiss Supra 40VP, Germany) at an accelerating voltage of  $15\text{ kV}$ . The micrographs were taken at magnifications of  $100\times$  to  $200\times$ . The exposed surface was coated with Au for 1 min before analyzed.

## 4. Results and discussion

The molecular structures of the respective liquid crystalline monomer, namely, RM257 and the cross-linking agent named PETMP used to polymerize liquid crystalline elastomer, are shown in Figure 1a. These two compositions were reacted using a DPA-based catalyst via a thiol-Michael addition reaction. This catalyst was responsible for accelerating the reaction between the electron-deficient vinyl groups of RM257 structures and the thiol groups of PETMP [36]. This reaction was completed after curing at room temperature for 24 h. For the ELC composites, Kraft lignin was physically mixed into the LCE system at 3, 5, and 7 wt%. Figure 1b displays the

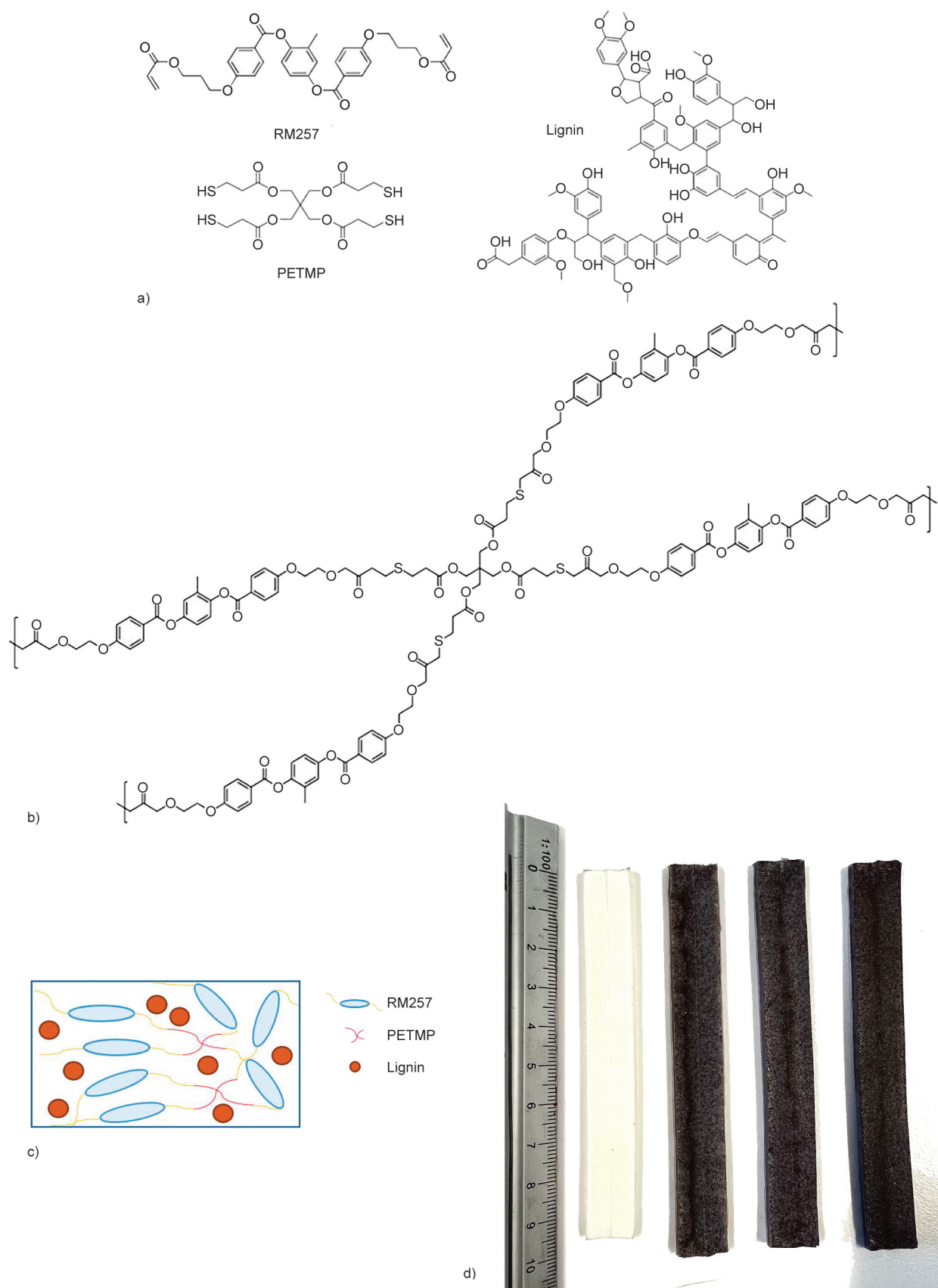


**Figure 1.** Molecular structures of RM257 monomers and a four-armed PETMP crosslinking agent (a); molecular structure of the crosslinked LCE (b); schematic of the ELC composites with lignin filler (c); an image of the LCE and ELC composite samples with Kraft lignin (d), from left to right; neat LCE, ELC composites with 3, 5, and 7 wt% lignin, respectively.

molecular structure of lignin utilized in this work, which is from a pulping process. The schematic of lignin-filled in ELC composites is shown in Figure 1c. In addition, the neat LCE and ELC composite samples with different weight ratios of Kraft lignin after completing the synthesis process are shown in Figure 1d.

#### 4.1. FTIR analysis

The FTIR spectra of Kraft lignin, LC monomers (RM257), neat LCE, and ELC composites were collected to study their chemical compositions. The FTIR spectrum of Kraft lignin was observed in Figure 2a. The broad peak at  $3215\text{ cm}^{-1}$  corresponds to the O–H stretching of hydrogen-bonded aromatic and aliphatic groups. The peaks observed at  $2934$  and  $1424\text{ cm}^{-1}$  correspond to the C–H stretching in methyl and methylene groups. The peaks at  $1592$  and  $1511\text{ cm}^{-1}$  correspond to aromatic ring vibration. The O–H vibration of phenolic groups is observed at  $1369\text{ cm}^{-1}$ . The peaks at  $1215$  and  $1029\text{ cm}^{-1}$  are attributed to vibration in the syringyl and guaiacyl structures [37]. The O–H stretching of secondary and primary alcohols is observed at  $1123$  and  $1079\text{ cm}^{-1}$ . The peak at  $853\text{ cm}^{-1}$  corresponds to the out-of-plane vibration of the C–H bond of aromatic deformation. These FTIR peaks of Kraft lignin are similar to those reported by Kong *et al.* [38] and Brazil *et al.* [39].

The FTIR spectra of LC monomers (RM257), LCE, and ELC composites with different Kraft lignin contents are divided into region 1 ( $3800$  to  $2200\text{ cm}^{-1}$ ) and region 2 ( $1800$  to  $400\text{ cm}^{-1}$ ), as illustrated in Figures 2b, 2c, and 2d. In region 1 (Figure 2b), the FTIR peaks of RM257 monomers and the LCE sample present a slight shift in the range of  $2992$  to  $2842\text{ cm}^{-1}$ . This is possibly due to the formation of inter- and intramolecular bonding of C–H stretching groups [37]. Figure 2c focuses in the range of  $3800$  to  $3000\text{ cm}^{-1}$  of the FTIR curve, where it can be observed that the FTIR peaks slightly intensifies in the region corresponding to stretching of the O–H groups, indicating contributions of hydrogen bonding due to further increase of the lignin in the composite. In region 2 (Figure 2d), the FTIR spectrum of LC monomers (RM257) exhibits a significant peak at  $808\text{ cm}^{-1}$ , corresponding to the out-of-plane vibration of the C–H bond of the acrylate group. While a  $1715\text{ cm}^{-1}$  peak relates to the C=O stretching of the mesogenic acrylate ester group. These peaks were similarly reported by Kamal and Park [13]. For the LCE sample, the peaks at  $1636$  and  $810\text{ cm}^{-1}$  disappear due to the interaction of acrylate groups of RM257 and thiol groups of PETMP. This interaction also reduces the height of a  $1411\text{ cm}^{-1}$  peak of the acrylate groups of the RM257 monomers. For the ELC composites, the FTIR spectrum

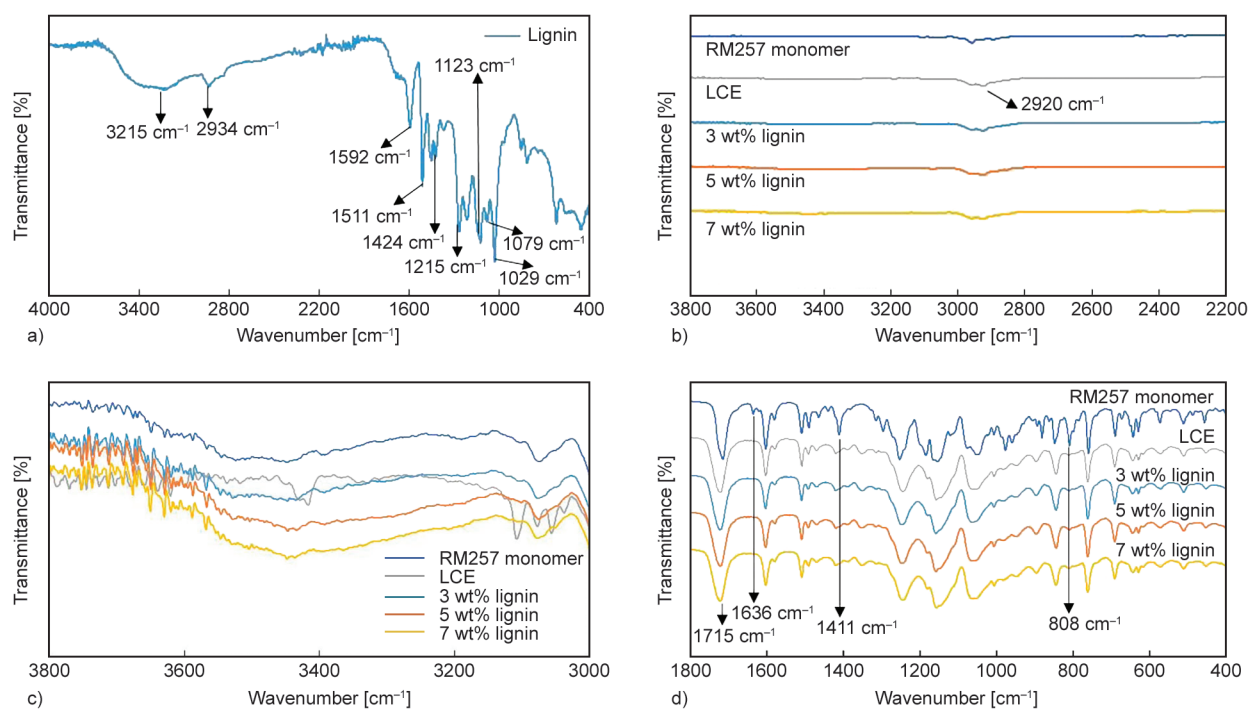


**Figure 2.** The FTIR spectra of Kraft lignin (a), and region 1 and region 2 of RM257 monomer, LCE and ELC composites from  $3800$  to  $2200\text{ cm}^{-1}$  (b),  $3800$  to  $3000\text{ cm}^{-1}$  (c), and  $1800$  to  $400\text{ cm}^{-1}$  (d).

of these samples with different lignin contents has no noticeable change compared to the neat LCE sample spectrum due to a small amount of lignin content filled in the LCE system.

#### 4.2. Thermal properties

DSC was utilized to study the thermal properties of the LC monomer, LCE, and ELC composites. Figure 3 shows the phase transitions of RM257 monomers with well-defined temperature changes. The monomers were heated first at a rate of  $5\text{ }^{\circ}\text{C}\cdot\text{min}^{-1}$  and then cooled at  $3\text{ }^{\circ}\text{C}\cdot\text{min}^{-1}$ . In the heating step, the heat flow of these monomers shows a minor endothermic peak at  $41\text{ }^{\circ}\text{C}$  and two significant peaks at  $76$  and  $128\text{ }^{\circ}\text{C}$ . The minor peak at  $41\text{ }^{\circ}\text{C}$  is attributed to a crystal-crystal phase transition of the monomers [40]. Meanwhile, the two significant peaks correspond to solid crystalline-nematic ( $T_{\text{CrN}}$ ) and nematic-isotropic ( $T_{\text{NI}}$ ) transition temperatures. These phase transition behaviors were previously reported by Kim *et al.* [40]. In addition, the exothermic peaks that occur in the cooling step at  $127$  and  $31\text{ }^{\circ}\text{C}$  correspond to  $T_{\text{NI}}$  and re-crystallization temperature, respectively. This figure depicts that the monomers can reorient their molecular structure from isotropic state to nematic-liquid crystal and solid crystalline states upon the change in the temperature.

Figure 4 depicts the DSC thermograms of LCE and ELC composites at various Kraft lignin contents

from 3 to 7 wt%. A neat LCE curve demonstrates a glass transition temperature ( $T_g$ ) at  $-4\text{ }^{\circ}\text{C}$  and  $T_{\text{NI}}$  at  $96\text{ }^{\circ}\text{C}$ . Meanwhile,  $T_g$  of the ELC composites increases with increasing Kraft lignin content. The observed enhancement in the  $T_g$  of the composites is because Kraft lignin has condensed rigid phenolic moieties that suppress the thermal mobility of the composite structures compared to neat LCE samples [41, 42]. However,  $T_{\text{NI}}$  of the ELC composites could not be detected by standard DSC due to its lower resolution, and hence these were determined from Tan delta under dynamic mechanical analysis to identify all the phase transitions. The values of  $T_g$  of neat LCE and all ELC composites are included in Table 1.

The thermal stability of the LCE and ELC composite samples was studied using thermogravimetric analysis (TGA). This property is defined as the ability of the polymers to resist heat and thermal decomposition upon an increase in temperature [43]. Figure 5 depicts the TGA and derivative thermogravimetric (DTG) thermograms of the neat LCE, Kraft lignin, and the ELC composites with 3, 5, and 7 wt% lignin contents. From the thermograms, the TGA curve of the Kraft lignin exhibits a slight decrease at approximately  $100\text{ }^{\circ}\text{C}$  due to the water evaporation. The significant degradation of this biomaterial occurs in the temperature range of  $100$  and  $550\text{ }^{\circ}\text{C}$ . The maximum weight loss from a DTG curve is  $436\text{ }^{\circ}\text{C}$ , which is suggested to be due to the fragmentation of

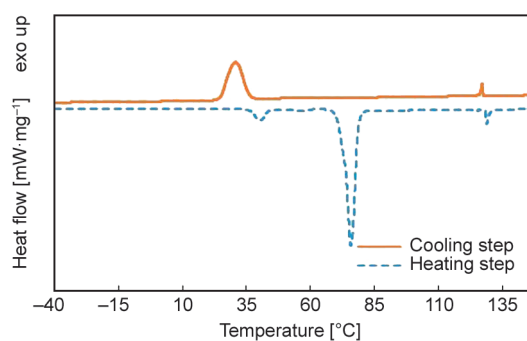


Figure 3. DSC thermogram of liquid crystalline monomer (RM257).

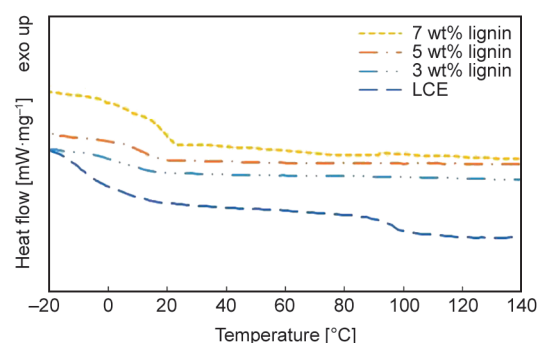
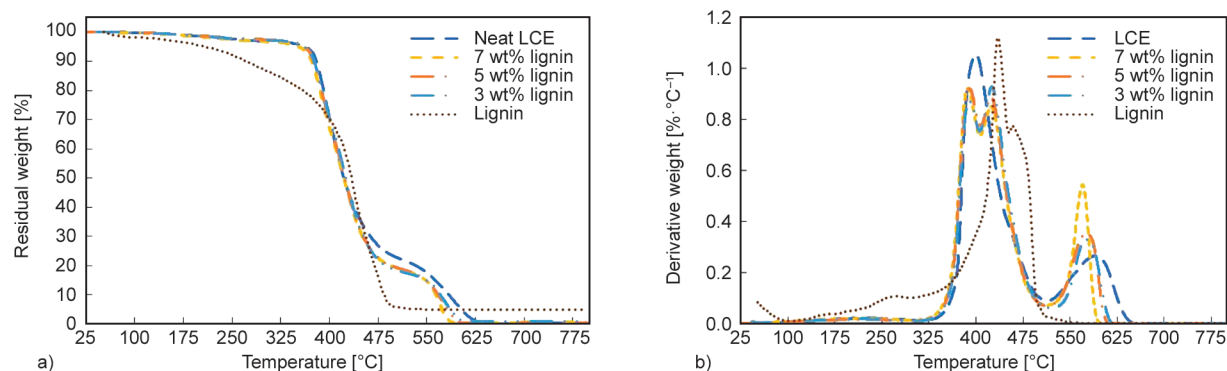


Figure 4. DSC thermograms of liquid crystalline elastomer (LCE) and ELC composites with different mass ratios of Kraft lignin.

Table 1. DSC and DMA results of LCE and ELC composites at various weight ratios of Kraft lignin.

Samples	DSC		DMA		
	$T_g$ [°C]	$T_{\text{NI}}$ [°C]	$T_{\text{NI}}$ [°C]	$E'$ at $25\text{ }^{\circ}\text{C}$ [MPa]	$E'$ at $110\text{ }^{\circ}\text{C}$ [MPa]
Neat LCE	-4	96	97	6.5	0.3
ELC composites + 3wt% lignin	4	–	78	11.9	1.0
ELC composites + 5wt% lignin	11	–	86	14.2	1.7
ELC composites + 7wt% lignin	16	–	76	60.3	4.8



**Figure 5.** TGA (a) and DTG (b) thermograms of the LCEs, Kraft lignin, and ELC composites with different lignin content, tested in air.

carbohydrates, aromatic rings, and inter-linkages releasing phenols into a vapor phase [39, 44]. Meanwhile, the residual weight of lignin at 700 °C is approximately 4.8%.

The neat LCE sample indicates two maximum peaks at 403 and 591 °C, relating to a two-step degradation. The first peak corresponds to the fragmentation of aliphatic chains in the LCE structure. However, the second peak relates to the degradation of aromatic rings in a mesogens segment. For ELC composites with 3 to 7 wt% Kraft lignin content, three distinct steps of degradation are observed in the DTG curve. The peaks at 392 and 580 °C are the degradation of aliphatic chains and mesogens of LCE, respectively. Meanwhile, the DTG peak at 431 °C is the fragmentation of Kraft lignin in the composite samples. From these thermograms, incorporating Kraft lignin into the LCE matrix barely affects an improvement in the thermal stability of the composites. The ELC composites exhibit their thermal properties similar to the neat LCE samples.

### 4.3. Dynamic mechanical properties

Storage modulus ( $E'$ ) and  $\tan \delta$  of LCE and ELC composites were investigated using a DHR in the tensile mode. Figure 6 shows the storage modulus ( $E'$ ) of the LCE and ELC composites as a function of temperature. The results show that the LCE has two thermal relaxations identified as glass transition temperature ( $T_g$ ) and nematic-isotropic temperature ( $T_{NI}$ ). These transition temperatures manifest the changes in the chain mobility and orientational order of the LCE and ELC composite structures. In the nematic state, the  $E'$  at above  $T_g$  dramatically drops to a lower modulus value due to the internal nematic director ( $\bar{n}$ ) relaxation modes of the orientational order of the LCE structures [45]. Above this point, the  $E'$  shows

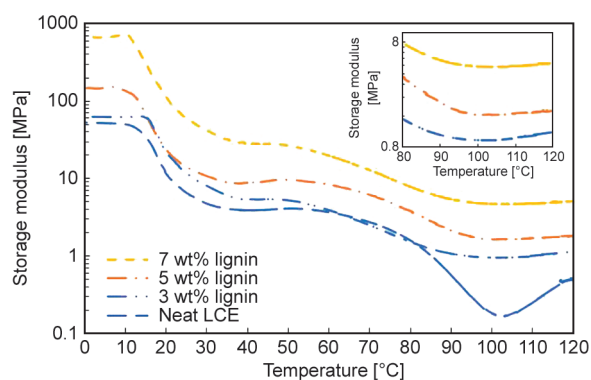


**Figure 6.** Storage modulus ( $E'$ ) of LCE and ELC composites with various lignin contents.

a minimum corresponding to  $T_{NI}$ . In the isotropic phase, the  $E'$  shows an upturn due to the entropic rubber elasticity of the LCE [45].

For the composite samples, the  $E'$  curves show similar trends in thermal relaxations to that of the neat LCE. It, therefore, seems that the amount of Kraft lignin has no dramatic effects on the orientational and positional orders of the LCE structures at elevated temperatures. However, in absolute terms, Kraft lignin content significantly increases the storage modulus ( $E'$  values) of the ELC composites in both nematic and isotropic states at 25 and 110 °C. The results show that the  $E'$  of the neat LCE at these states are 6.5 and 0.3 MPa, respectively. The  $E'$  of the composites increases upon the addition of Kraft lignin by approximately an order of magnitude at nematic state and well above that at isotropic states summarized in Table 1. This enhancement in the storage modulus in the composites compared to neat LCE was expected as the rigid aromatic structures of lignin increase the stiffness of the composite structures [33, 46].

$\tan \delta$  of LCE and ELC composite samples are shown in Figure 7.  $\tan \delta$  is the ratio of energy dissipated

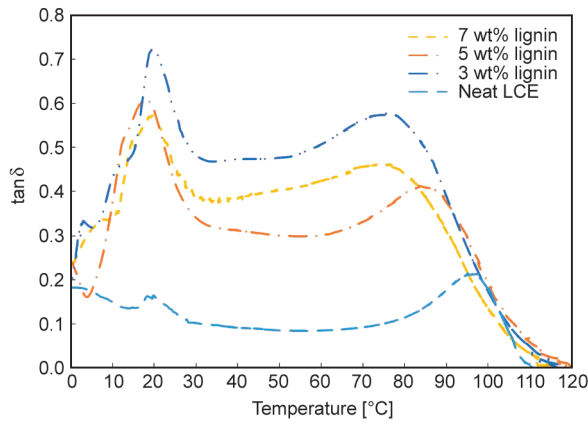


Figure 7. Tan  $\delta$  of neat LCE and ELC composites at various lignin contents.

per cycle of sinusoidal deformation (loss modulus,  $E''$ ) over the storage modulus,  $E'/E'$ . From the diagram, the overall trend in tan delta curves of all composite samples is similar to the neat LCE. They exhibit two distinct peaks at different temperature regions. The first peak corresponds to  $T_g$ , and the second peak is defined as  $T_{NI}$ . For shape memory applications,  $T_{NI}$  is typically used as the switching temperature between the original and temporary shapes because this temperature is commonly higher than the room temperature and hence less sensitive to changes in the ambient conditions. Table 1 also summarizes the  $T_{NI}$  of all samples, and it can be observed that incorporating lignin into the LCE reduces this temperature. As the temperature increases, the kinetic energy of the structural unit in both lignin and LCE rises, which results in both increased overall free volume and enhanced mobility of the molecules in LCE matrix and the lignin filler. This is the possible driving factor for the further interaction between the functional groups of the two polymers. With the increased interaction, and perhaps through diffusion-based mechanism, the rigid lignin structure

seems to disrupt the orientational order of the LCE structure and hence the earlier observed onset of nematic to isotropic transition in the LCE composites.

#### 4.4. Shape memory properties

Shape memory properties of the LCE and ELC composites, including  $R_f$  and  $R_r$ , were characterized by a DHR in tensile mode. The samples were deformed and recovered via a thermal-induced process using  $T_{NI}$  as a switching temperature. The  $R_f$  is the ability to maintain a temporary shape of the samples after unloading at a low temperature. The  $R_r$  relates to the recoverability of the samples to their original shape upon being reheated to an elevated temperature. The values of these two key shape memory properties were calculated by Equations (1) and (2). Figure 8 illustrates changes in the strain of the neat LCE and 3 wt% Kraft lignin ELC composites in various steps of the shape memory process. The results show that the  $R_f$  of the neat LCE sample is 91.2%. Meanwhile, the LCE exhibits an excellent  $R_r$ , approximately 99.7%. For the ELC composites, the  $R_f$  significantly improved with increasing Kraft lignin content, as indicated in Table 2, where composites show an  $R_f$  of nearly 100%. It is suggested that the aromatic structures of lignin with strong intermolecular hydrogen bonding can enhance the netpoints density in the composite system, leading to an improved  $R_f$  of the composite samples [30, 47].

Table 2. Shape memory properties of the neat LCE and ELC composites.

	Samples			
	Neat LCE	ELC composites + 3 wt% lignin	ELC composites + 5 wt% lignin	ELC composites + 7 wt% lignin
$R_f$ [%]	91.2	95.6	94.7	97.0
$R_r$ [%]	99.7	99.5	99.8	99.6

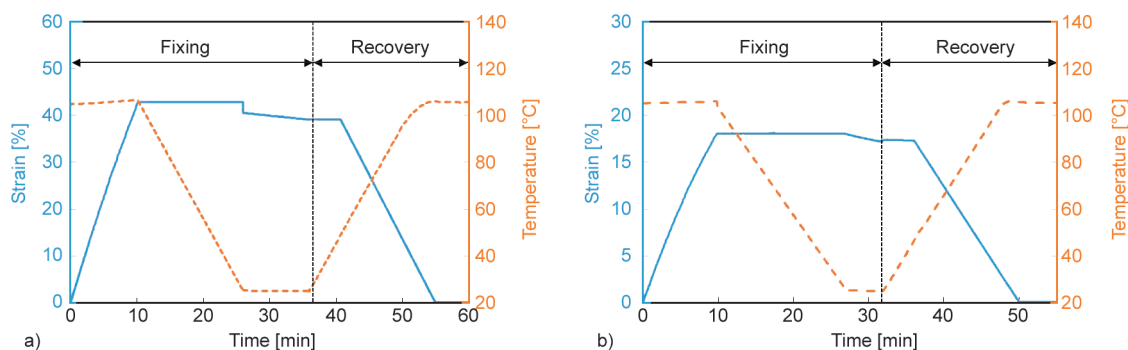
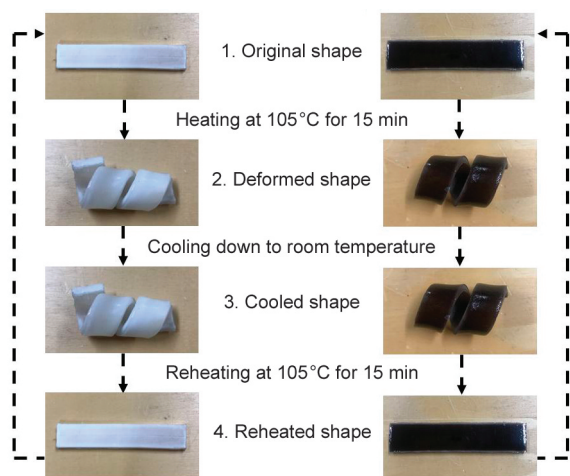


Figure 8. Changes in the strain as a function of the temperature of neat LCE sample (a) and ELC composite with 3 wt% lignin (b) via the thermomechanical shape memory process.



**Figure 9.** Steps of the thermomechanical shape memory process of LCE and 7 wt% lignin-ELC composites.

Figure 9 illustrates the steps taken during the thermomechanical shape memory process for the cases of neat LCE and ELC composites with 7 wt% lignin. A rectangular shape of various samples was first heated at 105 °C for 15 min by a heat gun. Then, the sample was manually deformed to a curled shape at this temperature. It is then cooled down to room temperature to maintain the temporary shape in this step. In the recovery step, the curl-shaped sample was reheated at 105 °C, resulting in a gradual recovery of the sample to its original rectangular shape. As a comparison, the shape memory behavior of the composite samples was also studied through a similar thermal-induced process, which turned out to be similar to the neat LCEs; however, the recovery time is faster than the neat LCE sample.

To evaluate the recovery time of LCE and ELC composite samples at a well-defined temperature, we measured their recovery angle over time through the following protocol. The rectangular-shaped samples with 3 mm thickness were deformed to a U-shape at 105 °C (above their  $T_{NI}$ ). The samples were then cooled down to room temperature to fix this shape. The samples were placed in an oven, and their shape recovery behavior over time was quantified through readings of a degree protractor set inside the oven (see Figure 11). The initial U-shape of the samples was set as 0° on the protector. A video camera recorded the recovery angle of the samples as a function of time at 105 °C until the samples recovered to a rectangular shape (180°).

Figure 10 shows the recovery angles of all the samples as a function of time. It further shows that the angle of the neat LCE sample initiates its recovery

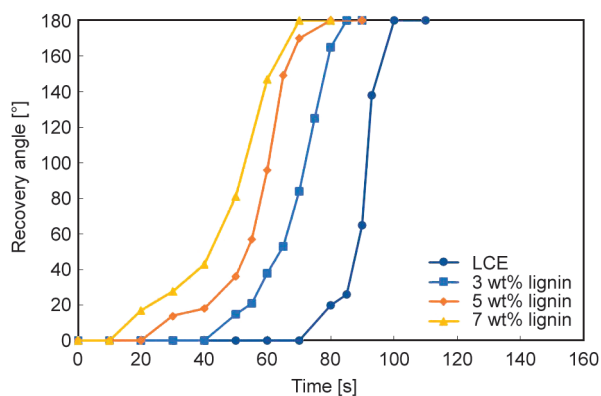


**Figure 10.** Recovery angle of the neat LCE and ELC composites with various lignin contents as a function of time.

at 70 s and fully recovers at 100 s. In addition, the presence of Kraft lignin content reduces the recovery time of the composite samples. The ELC composites with 3, 5, and 7 wt% Kraft lignin start to recover at 40, 20, and 10 s, respectively. Eventually, all-composite samples recover to a rectangular shape within 85, 75, and 70 s, respectively. These results further suggest that lignin operates as extra netpoints or hard segments in the shape memory mechanism, leading to an enhanced ability to store a higher degree of elastic energy during the deformation process [48]. The release of this energy during the recovery process associated with the mobility of the flexible tails of the LCE structure enables the ELC composites to recover faster than the neat LCE.

Figure 11 illustrates a series of screenshots of the recovery behavior of all LCE and ELC composites at various times through their recovery process at 105 °C. It is observed that lignin improves the recoverability of the ELC composite samples compared to the neat LCE.

#### 4.5. Scanning electron microscopy (SEM)

The surface morphology of the 7 wt% lignin ELC composites fracture was studied using SEM analysis with magnifications of 100× to 200×. This analysis allows the investigation of the dispersion of Kraft lignin particles in the LCE matrix. Figure 12 illustrates that the Kraft lignin particles are spherical and embedded within the matrix. In this case, the spherical shape of Kraft lignin is necessary for its isotropic reinforcement [49]. The Kraft lignin is liable to agglomerate in the LCE matrix due to the stronger cohesion and weaker adhesion forces to the phenolic structures between the lignin particles [50]. The particles further exhibit a large scatter in the particle

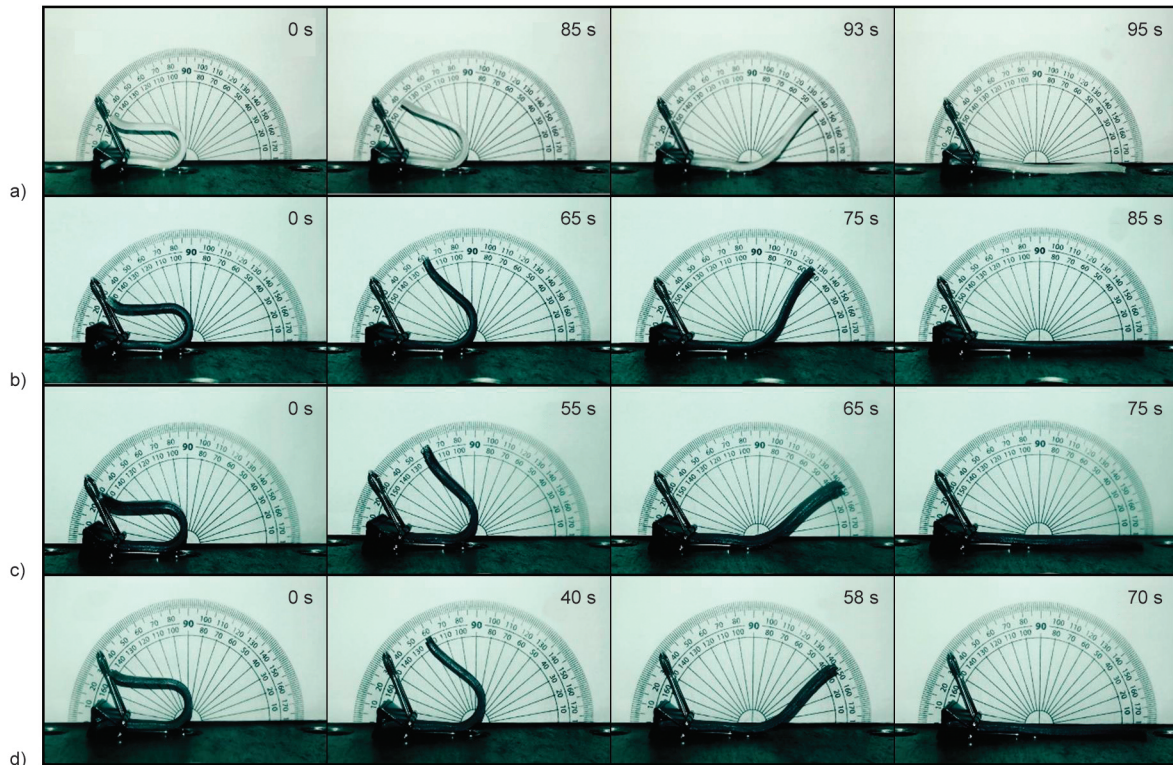


**Figure 11.** Screenshots of recovery angle at various times during the recovery process of LCE and ELC composites at 105 °C, recorded by a video camera; a) neat LCE, b) ELC composite with 3 wt% lignin, c) ELC composite with 5 wt% lignin, and d) ELC composite with 7 wt% lignin.

size range, which is mainly 20 to 100  $\mu\text{m}$ . From this figure, even though the lignin particles exhibit poor dispersion and no surface modification, this filler can improve the properties of the composite samples. It can be confirmed by the DMA results that an addition of Kraft lignin content improves the storage modulus of the ELC composites compared with the neat LCE counterpart. In this case, the lignin particles are responsible for the rigid reinforcing phase due to their high stiffness.

For shape memory applications, Kraft lignin distributes throughout the LCE matrix, allowing an increase in the netpoints density in the composite structures. Furthermore, the ability to hydrogen bonding of this filler with other molecular structures contributes to the netpoints density of the composites [47]. Thus, the addition and distribution of this biomaterial in the LCE samples can improve the shape memory characteristics, including  $R_f$  as well as recovery time of the ELC composites based on RM257.

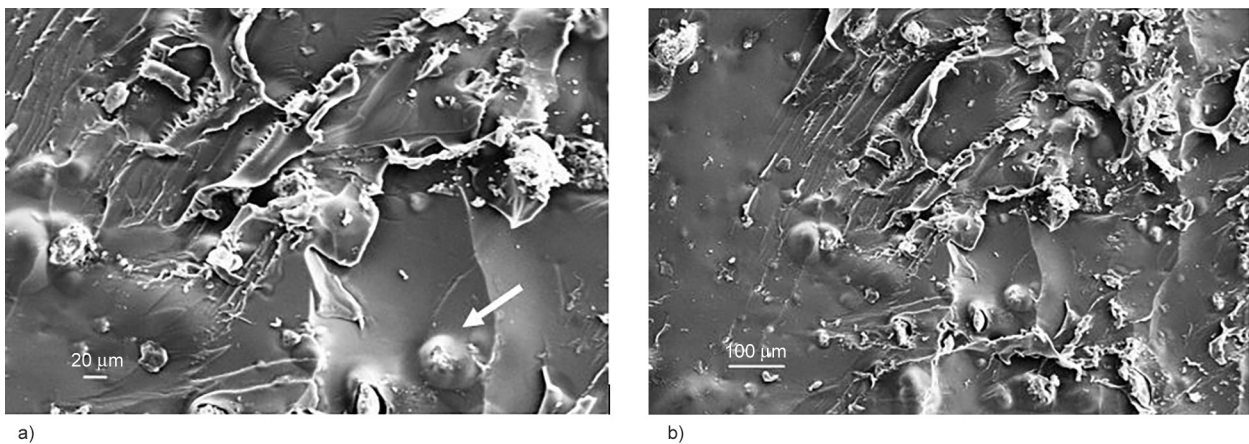


**Figure 12.** SEM fractured surface of ELC composites with 7 wt% lignin at 20  $\mu\text{m}$  (a) and 100  $\mu\text{m}$  (b). Arrows point out lignin particles.

## 5. Conclusions

In this work, we successfully fabricated new diacrylate mesogen-based ELC composites with Kraft lignin as the biobased filler for shape memory applications. The results of the lignin-ELC composites indicate excellent  $R_f$  via a thermomechanical shape memory process of nearly 100%. Specifically, the addition of lignin improves the  $R_f$  of the ELC composites in the range of 94.% to 97.0% upon its addition in the range 3 to 7 wt%, respectively. This bio-material can also reduce the recovery time of the composites when heated at a high temperature. The 7 wt% lignin composites could fully recover within 70 s, while the neat LCE sample showed a full recovery in 100 s.

Lignin-ELC composites as a novel combination, provide an excellent opportunity to develop more sustainable shape memory composite materials, given that they can be obtained from renewable resources and are abundant in nature. Lignin offers versatile chemistry due to its intrinsic structural aromatic compounds available through functional groups, viz. p-coumaryl, coniferyl, and syringyl alcohol.

Furthermore, the presence of Kraft lignin imparts improved dynamic mechanical properties in the composites by especially promoting the storage modulus as a key indicator of structures' true stiffness. The tendency of lignin particles to form spherical agglomerates at a macroscopic scale provides for an isotropic reinforcing effect in the ELC composites while enhancing the shape memory characteristics of the resultant composites.

The overall improved thermal and mechanical stabilities of the ELC composite improve the robustness of the applications where these are employed and hence enhance their long-term durability against environments exerting high thermal and mechanical stresses. Based on these results, the lignin-ELC composites have the potential to enable more sustainable applications of shape memory elastomeric composites in a variety of industrial environments for smart sensing and actuations such as soft robotics, smart actuators and sensors, and high-end space engineering.

## Acknowledgements

P. Prathumrat would like to acknowledge Premika Govindaraj of Swinburne University of Technology for her initial assistance on the HR-1 DHR training.

## References

- [1] Gong X., Tan K., Deng Q., Shen S.: Athermal shape memory effect in magnetoactive elastomers. *ACS Applied Materials and Interfaces*, **12**, 16930–16936 (2020). <https://doi.org/10.1021/acsami.0c01453>
- [2] Lai S.-M., Wang X.-F.: Shape memory properties of olefin block copolymer (OBC)/poly( $\epsilon$ -caprolactone) (PCL) blends. *Journal of Applied Polymer Science*, **134**, 45475 (2017). <https://doi.org/10.1002/app.45475>
- [3] Ramaraju H., Ul-Haque A., Verga A. S., Bocks M. L., Hollister S. J.: Modulating nonlinear elastic behavior of biodegradable shape memory elastomer and small intestinal submucosa(SIS) composites for soft tissue repair. *Journal of the Mechanical Behavior of Biomedical Materials*, **110**, 103965 (2020). <https://doi.org/10.1016/j.jmbbm.2020.103965>
- [4] Chen Z., Li Y., Yao C.: Biomass shape memory elastomers with rapid self-healing properties and high recyclability. *Biomacromolecules*, **22**, 2768–2776 (2021). <https://doi.org/10.1021/acs.biomac.1c00465>
- [5] Zhang Y., Hu Q., Yang S., Wang T., Sun W., Tong Z.: Unique self-reinforcing and rapid self-healing polyampholyte hydrogels with a pH-induced shape memory effect. *Macromolecules*, **54**, 5218–5228 (2021). <https://doi.org/10.1021/acs.macromol.0c02657>
- [6] Prathumrat P., Tiptipakorn S., Rimdusit S.: Multiple-shape memory polymers from benzoxazine–urethane copolymers. *Smart Materials and Structures*, **26**, 065025 (2017). <https://doi.org/10.1088/1361-665X/aa6d47>
- [7] Salaeh S., Das A., Wießner S.: Design and fabrication of thermoplastic elastomer with ionic network: A strategy for good performance and shape memory capability. *Polymer*, **223**, 123699 (2021). <https://doi.org/10.1016/j.polymer.2021.123699>
- [8] Prathumrat P., Nikzad M., Hajizadeh E., Arablouei R., Sbarski I.: Shape memory elastomers: A review of synthesis, design, advanced manufacturing, and emerging applications. *Polymers for Advanced Technologies*, **33**, 1782–1808 (2022). <https://doi.org/10.1002/pat.5652>
- [9] Xiao X., Hu J., Gui X., Qian K.: Shape memory investigation of  $\alpha$ -keratin fibers as multi-coupled stimuli of responsive smart materials. *Polymers*, **9**, 87 (2017). <https://doi.org/10.3390/polym9030087>
- [10] Behl M., Lendlein A.: Shape-memory polymers. *Materials Today*, **10**, 20–28 (2007). [https://doi.org/10.1016/S1369-7021\(07\)70047-0](https://doi.org/10.1016/S1369-7021(07)70047-0)
- [11] Lendlein A., Behl M., Hiebl B., Wischke C.: Shape-memory polymers as a technology platform for biomedical applications. *Expert Review of Medical Devices*, **7**, 357–379 (2010). <https://doi.org/10.1586/erd.10.8>

- [12] Michal B. T., McKenzie B. M., Felder S. E., Rowan S. J.: Metallo-, thermo-, and photoresponsive shape memory and actuating liquid crystalline elastomers. *Macromolecules*, **48**, 3239–3246 (2015).  
<https://doi.org/10.1021/acs.macromol.5b00646>
- [13] Kamal T., Park S-Y.: Shape-responsive actuator from a single layer of a liquid-crystal polymer. *ACS Applied Materials and Interfaces*, **6**, 18048–18054 (2014).  
<https://doi.org/10.1021/am504910h>
- [14] Lee K. M., Koerner H., Vaia R. A., Bunning T. J., White T. J.: Light-activated shape memory of glassy, azobenzene liquid crystalline polymer networks. *Soft Matter*, **7**, 4318–4324 (2011).  
<https://doi.org/10.1039/C1SM00004G>
- [15] Beyer P., Zentel R.: Photoswitchable smectic liquid-crystalline elastomers. *Macromolecular Rapid Communications*, **26**, 874–879 (2005).  
<https://doi.org/10.1002/marc.200500093>
- [16] Yu Y., Nakano M., Ikeda T.: Directed bending of a polymer film by light. *Nature*, **425**, 145 (2003).  
<https://doi.org/10.1038/425145a>
- [17] Prathumrat P., Sbarski I., Hajizadeh E., Nikzad M.: A comparative study of force fields for predicting shape memory properties of liquid crystalline elastomers using molecular dynamic simulations. *Journal of Applied Physics*, **129**, 155101 (2021).  
<https://doi.org/10.1063/5.0044197>
- [18] Lee K. M., Bunning T. J., White T. J.: Autonomous, hands-free shape memory in glassy, liquid crystalline polymer networks. *Advanced Materials*, **24**, 2839–2843 (2012).  
<https://doi.org/10.1002/adma.201200374>
- [19] Burke K. A., Mather P. T.: Soft shape memory in main-chain liquid crystalline elastomers. *Journal of Materials Chemistry*, **20**, 3449–3457 (2010).  
<https://doi.org/10.1039/B924050K>
- [20] Traugott N. A., Volpe R. H., Bollinger M. S., Saed M. O., Torbati A. H., Yu K., Dadivanyan N., Yakacki C. M.: Liquid-crystal order during synthesis affects main-chain liquid-crystal elastomer behavior. *Soft Matter*, **13**, 7013–7025 (2017).  
<https://doi.org/10.1039/C7SM01405H>
- [21] Guin T., Settle M. J., Kowalski B. A., Auguste A. D., Beblo R. V., Reich G. W., White T. J.: Layered liquid crystal elastomer actuators. *Nature Communications*, **9**, 2531 (2018).  
<https://doi.org/10.1038/s41467-018-04911-4>
- [22] Wen Z., McBride M. K., Zhang X., Han X., Martinez A. M., Shao R., Zhu C., Visvanathan R., Clark N. A., Wang Y., Yang K., Bowman C. N.: Reconfigurable LC elastomers: Using a thermally programmable monodomain to access two-way free-standing multiple shape memory polymers. *Macromolecules*, **51**, 5812–5819 (2018).  
<https://doi.org/10.1021/acs.macromol.8b01315>
- [23] Rousseau I. A., Mather P. T.: Shape memory effect exhibited by smectic-C liquid crystalline elastomers. *Journal of the American Chemical Society*, **125**, 15300–15301 (2003).  
<https://doi.org/10.1021/ja039001s>
- [24] Tokumoto H., Zhou H., Takebe A., Kamitani K., Kojio K., Takahara A., Bhattacharya K., Urayama K.: Probing the in-plane liquid-like behavior of liquid crystal elastomers. *Science Advances*, **7**, eabe9495 (2021).  
<https://doi.org/10.1126/sciadv.abe9495>
- [25] Yu O., Kim K. H.: Lignin to materials: A focused review on recent novel lignin applications. *Applied Sciences*, **10**, 4626 (2020).  
<https://doi.org/10.3390/app10134626>
- [26] Norberg I., Nordström Y., Drouge R., Gellerstedt G., Sjöholm E.: A new method for stabilizing softwood kraft lignin fibers for carbon fiber production. *Journal of Applied Polymer Science*, **128**, 3824–3830 (2013).  
<https://doi.org/10.1002/app.38588>
- [27] Zong E., Liu X., Liu L., Wang J., Song P., Ma Z., Ding J., Fu S.: Graft polymerization of acrylic monomers onto lignin with  $\text{CaCl}_2\text{-H}_2\text{O}_2$  as initiator: Preparation, mechanism, characterization, and application in poly(lactic acid). *ACS Sustainable Chemistry and Engineering*, **6**, 337–348 (2018).  
<https://doi.org/10.1021/acssuschemeng.7b02599>
- [28] Nisha S. S., Nikzad M., Al Kobaisi M., Truong V. K., Sbarski I.: The role of ionic-liquid extracted lignin micro/nanoparticles for functionalisation of an epoxy-based composite matrix. *Composites Science and Technology*, **174**, 11–19 (2019).  
<https://doi.org/10.1016/j.compscitech.2019.02.009>
- [29] Sternberg J., Pilla S.: Materials for the biorefinery: High bio-content, shape memory kraft lignin-derived non-isocyanate polyurethane foams using a non-toxic protocol. *Green Chemistry*, **22**, 6922–6935 (2020).  
<https://doi.org/10.1039/D0GC01659D>
- [30] Chen S., Liu J.: Liquid metal enabled unconventional heat and flow transfer. *ES Energy and Environment*, **5**, 8–21 (2019).  
<https://doi.org/10.30919/eseec8c318>
- [31] Liu L-Y., Karaaslan M. A., Hua Q., Cho M., Chen S., Rennecker S.: Thermo-responsive shape-memory polyurethane foams from renewable lignin resources with tunable structures–properties and enhanced temperature resistance. *Industrial and Engineering Chemistry Research*, **60**, 11882–11892 (2021).  
<https://doi.org/10.1021/acs.iecr.1c01717>
- [32] Xu Y., Odelius K., Hakkarainen M.: One-pot synthesis of lignin thermosets exhibiting widely tunable mechanical properties and shape memory behavior. *ACS Sustainable Chemistry and Engineering*, **7**, 13456–13463 (2019).  
<https://doi.org/10.1021/acssuschemeng.9b02921>
- [33] Nguyen N. A., Meek K. M., Bowland C. C., Naskar A. K.: Responsive lignin for shape memory applications. *Polymer*, **160**, 210–222 (2019).  
<https://doi.org/10.1016/j.polymer.2018.11.055>

- [34] Sivasankarapillai G., Li H., McDonald A. G.: Lignin-based triple shape memory polymers. *Biomacromolecules*, **16**, 2735–2742 (2015).  
<https://doi.org/10.1021/acs.biomac.5b00655>
- [35] Likitaporn C., Mora P., Tiptipakorn S., Rimdusit S.: Recovery stress enhancement in shape memory composites from silicon carbide whisker-filled benzoxazine-epoxy polymer alloy. *Journal of Intelligent Material Systems and Structures*, **29**, 388–396 (2018).  
<https://doi.org/10.1177/1045389x17708041>
- [36] Nair D. P., Podgórski M., Chatani S., Gong T., Xi W., Fenoli C. R., Bowman C. N.: The thiol-michael addition click reaction: A powerful and widely used tool in materials chemistry. *Chemistry of Materials*, **26**, 724–744 (2014).  
<https://doi.org/10.1021/cm402180t>
- [37] de Freitas A. d. S., Rodrigues J. S., Maciel C. C., Pires A. A., Lemes A. P., Ferreira M., Botaro V. R.: Improvements in thermal and mechanical properties of composites based on thermoplastic starch and kraft lignin. *International Journal of Biological Macromolecules*, **184**, 863–873 (2021).  
<https://doi.org/10.1016/j.ijbiomac.2021.06.153>
- [38] Kong F., Wang S., Gao W., Fatehi P.: Novel pathway to produce high molecular weight kraft lignin–acrylic acid polymers in acidic suspension systems. *RSC Advances*, **8**, 12322–12336 (2018).  
<https://doi.org/10.1039/C7RA12971H>
- [39] Brazil T. R., Costa R. N., Massi M., Rezende M. C.: Structural, morphological, and thermal characterization of kraft lignin and its charcoals obtained at different heating rates. *Materials Research Express*, **5**, 045502 (2018).  
<https://doi.org/10.1088/2053-1591/aab7c2>
- [40] Kim N., Li Q., Kyu T.: Effect of trans-cis photoisomerization on phase equilibria and phase transition of liquid-crystalline azobenzene chromophore and its blends with reactive mesogenic diacrylate. *Physical Review E*, **83**, 031702 (2011).  
<https://doi.org/10.1103/PhysRevE.83.031702>
- [41] Gordobil O., Delucis R., Egüés I., Labidi J.: Kraft lignin as filler in PLA to improve ductility and thermal properties. *Industrial Crops and Products*, **72**, 46–53 (2015).  
<https://doi.org/10.1016/j.indcrop.2015.01.055>
- [42] Chung Y-L., Olsson J. V., Li R. J., Frank C. W., Waymouth R. M., Billington S. L., Sattely E. S.: A renewable lignin–lactide copolymer and application in bio-based composites. *ACS Sustainable Chemistry and Engineering*, **1**, 1231–1238 (2013).  
<https://doi.org/10.1021/sc4000835>
- [43] Charles J., Ramkumaar G. R., Azhagiri S., Gunasekaran S.: FTIR and thermal studies on nylon-66 and 30% glass fibre reinforced nylon-66. *E-Journal of Chemistry*, **6**, 909017 (2009).  
<https://doi.org/10.1155/2009/909017>
- [44] Tejado A., Peña C., Labidi J., Echeverria J. M., Mondragon I.: Physico-chemical characterization of lignins from different sources for use in phenol–formaldehyde resin synthesis. *Bioresource Technology*, **98**, 1655–1663 (2007).  
<https://doi.org/10.1016/j.biortech.2006.05.042>
- [45] Saed M. O., Elmadih W., Terentjev A., Chronopoulos D., Williamson D., Terentjev E. M.: Impact damping and vibration attenuation in nematic liquid crystal elastomers. *Nature communications*, **12**, 6676 (2021).  
<https://doi.org/10.1038/s41467-021-27012-1>
- [46] Kargarzadeh H., Galeski A., Pawlak A.: PBAT green composites: Effects of kraft lignin particles on the morphological, thermal, crystalline, macro and micromechanical properties. *Polymer*, **203**, 122748 (2020).  
<https://doi.org/10.1016/j.polymer.2020.122748>
- [47] Amini M., Hasheminejad K., Montazeri A.: Engineering the shape memory parameters of graphene/polymer nanocomposites through atomistic simulations: On the effect of nanofiller surface treatment. *Smart Materials and Structures*, **31**, 025010 (2021).  
<https://doi.org/10.1088/1361-665x/ac4194>
- [48] Liu Y., Zhang W., Zhang F., Leng J., Pei S., Wang L., Jia X., Cotton C., Sun B., Chou T-W.: Microstructural design for enhanced shape memory behavior of 4D printed composites based on carbon nanotube/poly(lactic acid) filament. *Composites Science and Technology*, **181**, 107692 (2019).  
<https://doi.org/10.1016/j.compscitech.2019.107692>
- [49] Hu L., Stevanovic T., Rodrigue D.: Compatibilization of kraft lignin-polyethylene composites using unreactive compatibilizers. *Journal of Applied Polymer Science*, **131**, 41040 (2014).  
<https://doi.org/10.1002/app.41040>
- [50] Klapiszewski L., Jamrozik A., Strzemiescka B., Matykiewicz D., Voelkel A., Jesionowski T.: Activation of magnesium lignosulfonate and kraft lignin: Influence on the properties of phenolic resin-based composites for potential applications in abrasive materials. *International Journal of Molecular Sciences*, **18**, 1224 (2017).  
<https://doi.org/10.3390/ijms18061224>